Electrospun single-walled carbon nanotube/polyvinyl alcohol composite nanofibers:

structure–property relationships

Electrospun single-walled carbon nanotube/polyvinyl alcohol composite nanofibers: structure–property relationships

Minoo Naebe[1], Tong Lin[1,4], Mark P Staiger[2], Liming Dai[3] and Xungai Wang[1]

[1] Centre for Material and Fibre Innovation, Deakin University, Geelong, VIC 3217, Australia
[2] Department of Mechanical Engineering, University of Canterbury, Christchurch, New Zealand
[3] Department of Chemical and Materials Engineering, The University of Dayton, Dayton, OH 45469, USA

E-mail: tong.lin@deakin.edu.au

Abstract
Polyvinyl alcohol (PVA) nanofibers and single-walled carbon nanotube (SWNT)/PVA composite nanofibers have been produced by electrospinning. An apparent increase in the PVA crystallinity with a concomitant change in its main crystalline phase and a reduction in the crystalline domain size were observed in the SWNT/PVA composite nanofibers, indicating the occurrence of a SWNT-induced nucleation crystallization of the PVA phase. Both the pure PVA and SWNT/PVA composite nanofibers were subjected to the following post-electrospinning treatments: (i) soaking in methanol to increase the PVA crystallinity, and (ii) cross-linking with glutaric dialdehyde to control the PVA morphology. Effects of the PVA morphology on the tensile properties of the resultant electrospun nanofibers were examined. Dynamic mechanical thermal analyses of both pure PVA and SWNT/PVA composite electrospun nanofibers indicated that SWNT–polymer interaction facilitated the formation of crystalline domains, which can be further enhanced by soaking the nanofiber in methanol and/or cross-linking the polymer with glutaric dialdehyde.

1. Introduction

With a one-dimensional hollow core at the nanometer scale, single-walled carbon nanotubes (SWNTs) have been widely used for developing new lightweight polymer composites with enhanced mechanical [1, 2], electrical [3, 4], and thermal properties [5, 6]. However, it is still a big challenge to fabricate SWNT/polymer composites with a uniform nanotube dispersion, controlled nanotube orientation, and improved nanotube–polymer interaction. While extensive studies have been conducted to improve the nanotube dispersion [5, 7–10] and to enhance the nanotube–polymer interaction, possible influences of the polymer morphology (e.g. crystallinity, cross-linking degree) on properties of the polymer and nanotube composites are much less discussed in the literature.

Electrospinning has recently been used to produce SWNT/polymer composite nanofibers [11–13]. As a result of the rapid fiber-drawing during electrospinning, the SWNTs with a high aspect-ratio tend to orientate along the axis of the electrospun fibers [12–15]. As such, the electrospun SWNT/polymer composite fibers generally exhibit improved mechanical and electrical properties. However, much of the work in the field has been focused on the preparation of electrospun nanofibers and subsequent characterization of their mechanical and electronic properties. A fundamental understanding of the carbon nanotube–polymer interaction within the composite nanofibers and its effect on the fiber properties is still lacking.

[4] Author to whom any correspondence should be addressed.

Having one hydroxyl group in each repeat unit, PVA is highly water-soluble and cross-linkable. By gel-spinning of SWNTs in PVA solution, SWNT/PVA fibers of a high toughness have been produced [2, 7, 16]. Recent studies indicated that SWNTs could initiate nucleation crystallization of PVA [1, 2, 17–24] to form a crystalline PVA layer around the nanotube surface with excellent mechanical properties. In our previous work [25], we have demonstrated that the addition of multi-walled carbon nanotubes (MWNTs) into an aqueous solution of PVA for electrospinning could lead to an increased PVA crystallinity in electrospun MWNT/PVA nanofibers produced even with an extremely rapid drawing and solidification process.

SWNTs differ from MWNTs in their size and dispersibility in solution and polymer matrix as well as mechanical and electronic properties. These differences justify further investigation into possible effects of SWNTs on the structure–property relationship of polymer electrospun nanofibers in the present study. For this purpose, we carried out electrospinning of SWNT/PVA composite nanofibers and investigated the influence of SWNTs on the PVA crystallinity within the electrospun composite nanofibers. As we shall see later, the nucleation crystallization of PVA in the composite nanofibers was confirmed by differential scanning calorimetry (DSC) and wide angle x-ray diffraction (WAXD). Post-electrospinning treatments with methanol or glutaric dialdehyde under appropriate conditions were used to change the PVA morphology (crystallinity and cross-linking degree), and hence tensile properties of the electrospun nanofibers. Dynamic mechanical thermal analysis (DMTA) was used to gain a better understanding of the nanotube–PVA interaction.

2. Experimental details

2.1. Materials

PVA ($Mw = 146\,000$–$186\,000$, 96% hydrolyzed) and all other chemicals were obtained from Aldrich-Sigma and used as received. SWNTs (purity 80%) were obtained from NNW New Materials Technology (China) and were purified by refluxing in 3N HNO_3 for 12 h prior to use.

2.2. Electrospinning of PVA nanofibers

SWNT/PVA nanofibers were prepared using a home-made electrospinning apparatus consisting of a plastic syringe with a metal syringe needle (21 Gauge), a syringe pump (KD Scientific), a high voltage power supply (ES30P, Gamma High Voltage Research), and a rotating metal drum collector. The distance between the tip of the needle and the collector was 15 cm. An aqueous solution of 11 wt% PVA containing 10 wt% SWNTs (by PVA weight) was used for the electrospinning under a flow rate of the polymer solution and an applied voltage of 0.6 ml h^{-1} and 18 kV, respectively. For comparison, pure PVA nanofibers were also electrospun from 11 wt% PVA solution under the same operating conditions.

2.3. Post-electrospinning fiber treatments

The resultant electrospun PVA nanofibers were subjected to the following two different post-electrospinning treatments:

(a) Methanol treatment: immersion in methanol for 24 h and then dried at 50 °C in air for 6 h;
(b) Cross-linking reaction: immersion in an acetone solution of 0.05 wt% glutaric dialdehyde for 4 h, and then cured at 150 °C in air for 10 min.

2.4. Characterization

The electrospun nanofibers were examined on scanning electron microscopy (SEM Leica S440). The fiber diameter was determined from SEM images with the aid of image analysis software (Image*Pro* + 4.5). Transmission electron microscope (TEM, JEM-200 CX JEOL) was used to observe the presence and morphology of carbon nanotubes with the electrospun nanofibers. Mechanical properties of the nanofiber mats were measured with a universal tensile tester (Lloyd LR30K), according to ASTM D-882. Differential scanning calorimetry (DSC) was performed using a Mettler-Toledo DSC 821 in an alternating mode at a heating rate of 10 °C min^{-1}. Wide angle x-ray diffraction (WAXD) was performed on a powder diffractometer (Philips 1140/90) using Cu radiation 1.54 Å. Water contact angles were measured on a goniometer (KSV CAM200 Instruments Ltd). Dynamic mechanical thermal analysis (DMTA) was performed on a Perkin Elmer Diamond DMTA in tension mode at frequencies of 1, 2, 4, 10 and 20 Hz at a heating rate of 2 °C min^{-1}.

3. Results and discussion

Figure 1 shows SEM images of the pure PVA and SWNT/PVA composite nanofibers, which are rather uniform in fiber diameters and free from any bead. The pure PVA nanofibers have an average diameter of 509 ± 97 nm, while their SWNT-containing counterparts are thinner with an average diameter of 315 ± 84 nm (table 1). The reduced fiber diameter for the SWNT/PVA nanofibers is presumably due to increased stretching of the fiber during electrospinning, as a result of increased charge when the conductive CNTs were present in the polymer solution. Upon the post-electrospinning treatment with methanol, the nanofibers showed a slight increase in the fiber diameter (table 1) whereas the cross-linking treatment caused the opposite effect (table 1). For the SWNT/PVA nanofibers, however, both post-electrospinning treatments led to a slight increase in the fiber diameter (figures 1(b) and (c)).

As shown in the TEM image in figure 2, the SWNTs were well dispersed in the polymer matrix. Most of the SWNTs oriented parallel or partially parallel to the axis of nanofiber, along with some other nonaligned bent short nanotubes. A few entangled nanotube structures were also observed in the nanofibers.

The post-electrospinning treatments were found to also cause changes in air/water contact angles. Water contact angles can be used as a measure of the surface hydrophobicity [26, 27]. The water contact angles for the
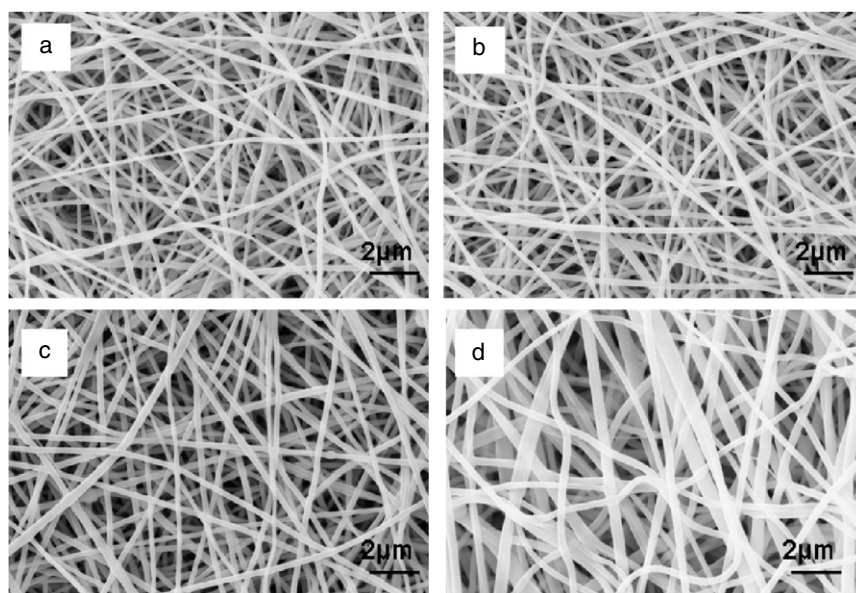
Figure 1. SEM micrographs of electrospun nanofibers. (a) Untreated SWNT/PVA nanofibers; (b) SWNT/PVA nanofibers treated by methanol, (c) cross-linked SWNT/PVA nanofibers, (d) neat PVA nanofibers (untreated).

Table 1. Fiber diameter, crystallinity, tensile properties and contact angle of PVA nanofiber mats.

| Post-treatments	Diameter (nm)	T_m (°C)	X_c (%)	Strength (MPa)	Strain (%)	Contact angle (deg)	T_g (°C)	$E_a(T_g)$ (kJ mol^{-1})	T_β (°C)	$E_a(T_\beta)$ (kJ mol^{-1})
				Pure PVA						
Control	509 ± 97	220	15.8	3.83	193.7	0	74	41.6	99	128.6
Methanol treated	520 ± 106	224	34.0	6.87	186.0	37.06	72	193.1	118	145.2
Cross-linked	499 ± 104	213	27.6	4.36	101.1	46.53	60	182.8	115	141.2
				SWNT/PVA						
Control	315 ± 84	224	37.0	5.91	119.9	29.61	71	115.9	114	133.4
Methanol treated	340 ± 63	222	74.7	9.23	116.4	48.61	71	164.9	126	161.4
Cross-linked	447 ± 61	215	17.9	6.02	90.4	83.15	73	144.5	126	153.7
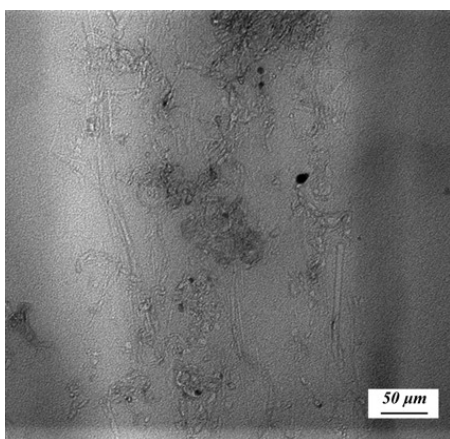
Figure 2. TEM image of a SWNT/PVA nanofiber.

pure PVA and the SWNT/PVA composite nanofiber mats before and after the post-electrospinning treatments are listed in table 1. Prior to the post-electrospinning treatment, contact angles of the pure PVA nanofibers cannot be recorded as the

water droplet was rapidly adsorbed into the highly hydrophilic PVA fibers. However, the methanol treatment increased the contact angle of the pure PVA nanofiber mat by about 37° (table 1). The contact angle for the cross-linked pure PVA nanofiber mat was even higher (~46°, table 1), attributable to the conversion of the hydrophilic –OH groups in PVA to acetal groups or ether linkages by cross-linking with glutaric dialdehyde [28]. The relatively high values of contact angles for the SWNT/PVA composite nanofibers with respect to their pure PVA counterparts indicated that the addition of SWNTs could reduce the number of –OH groups exposed on the surface of the composite nanofibers. Similar results have been previously reported for MWNT/PVA composite nanofibers [25].

Figure 3 shows DSC curves for the pure PVA and SWNT/PVA composite nanofibers before and after the post-electrospinning treatments. As can be seen, all of the nanofibers exhibited an endothermic peak around 212–225 °C, corresponding to the melting temperature of PVA (T_m). To investigate possible effects of the post-electrospinning effects on the crystallinity, we calculated the enthalpy ΔH values through numerical integration of areas covered by the melting
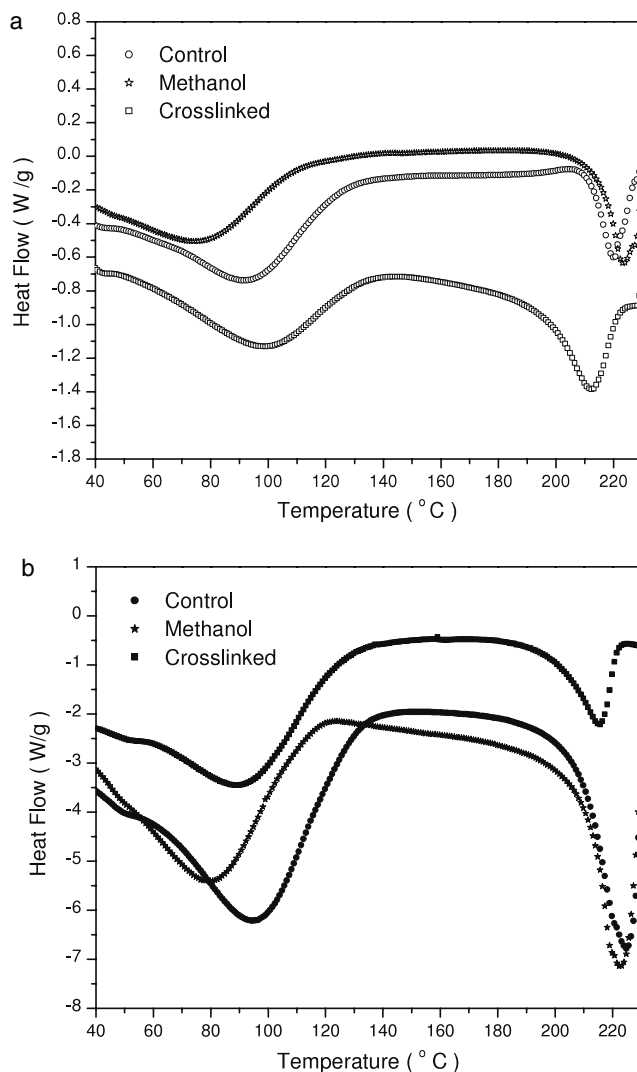
a

b

Figure 3. DSC curves of PVA and SWNT/PVA nanofibers.

Figure 4. WAXD patterns for PVA and SWNT/PVA nanofibers.

Table 2. Crystalline domain sizes of PVA in nanofibers

Post-treatments	Crystallite sizes (nm)	
	(001)	*(101)*
Pure PVA		
Control	87.5	30.5
Methanol treated	174.9	40.1
Cross-linked	88.6	33.1
SWNT/PVA		
Control	31.8	—
Methanol treated	33.3	—
Cross-linked	25.7	—

peak and normalized by sample mass. Using the enthalpy of 155 J g^{-1} for a theoretical 100% crystalline PVA as [18], we estimated that the pure PVA nanofibers exhibited a relatively low crystallinity of ∼15.8%, which increased to 34% and 27.6% for the methanol treated and cross-linked PVA nanofibers, respectively.

All of the SWNT/PVA composite nanofibers showed a higher crystallinity than their PVA counterparts. The SWNT/PVA nanofibers showed a crystallinity of 37% even before any post-treatment (table 1). The observed increase in the PVA crystallinity indicated that SWNTs promoted crystallization of PVA in the SWNT/PVA nanofibers. Similar observations have been reported for solution-cast SWNT/PVA films and wet-spun fibers [1, 18, 20, 22, 24].

WAXD was used to further study the PVA crystallization in both the pure PVA and SWNT/PVA composite nanofibers. As seen in figure 4, the diffraction peaks for the pure PVA nanofibers appeared at $2\theta = 19.4°$ and $16.1°$ characteristic of the (101) and (001) planes of semi-crystalline PVA, respectively [29, 30]. The (101) phase was the main crystalline due to the high integrated area.
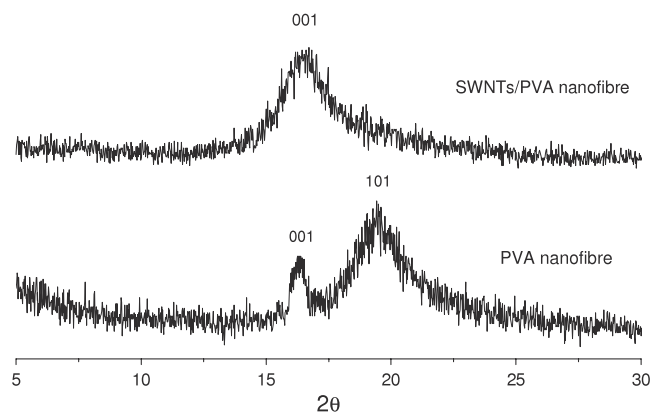
In contrast, the SWNT/PVA composite nanofibers showed only a single broad peak at $2\theta = 16.1°$, indicating a SWNT-induced change in the main crystalline phase of PVA from (101) to (001) due, most probably, to the confinement orientation of PVA macromolecular chains around the carbon nanotube surface within the nanofibers. The post-electrospinning treatments influenced diffraction patterns for both the pure PVA and SWNT/PVA composite nanofibers. For the pure PVA nanofibers, the methanol treatment led to a stronger (101) and weaker (001) reflection. On the other hand, the cross-linking treatment decreased both the (101) and (001) reflections of the pure PVA nanofibers. For the SWNT/PVA composite nanofibers, however, the post-electrospinning treatments had little influence on their diffraction patterns. This suggested that the presence of SWNTs stabilized the PVA crystallinity structure.

Based on the WAXD data, the crystalline domain size of PVA in the different electrospun nanofiber samples was calculated from the Scherrer equation [31] ($k = 0.9$) and listed in table 2. The crystalline domain size for both (101) and (001) phases in the pure PVA nanofibers was found to increase considerably after the methanol treatment. However, the cross-linking reaction caused only a slight increase in the crystalline domain size. For the SWNT-containing nanofibers, the PVA crystalline domain size was significantly smaller than that for the pure PVA nanofiber counterparts, though the crystallinity was much higher for the former. Compared to the untreated composite nanofibers, the (001) phase crystalline domain size

of the composite nanofibers slightly increased by the methanol treatment, but decreased upon cross-linking.

The above findings prompted us to investigate the influence of the post-electrospinning treatments on mechanical properties of the pure PVA and SWNT/PVA composite nanofibers. The tensile strength and strain to failure for the pure PVA nanofiber mat were measured to be 3.83 MPa and 193.7%, respectively. The methanol treatment was found to significantly increase the tensile strength, but slightly decrease the strain value. Like the methanol treatment, the cross-linking treatment also increased the tensile strength and lowered the strain to failure (table 1). Compared to the pure PVA nanofibers, all of the SWNT/PVA composite nanofibers possessed higher tensile strengths. Without any post-electrospinning treatment, the tensile strength of the SWNT/PVA composite nanofiber mat was 5.91 MPa or 54% higher than that of the pure PVA nanofiber. The strain to failure reduced to 119.9% for the SWNT/PVA composite nanofibers from 193.7% for the pure PVA nanofibers. The post-electrospinning treatments further improved the tensile strength for the SWNT/PVA composite nanofibers. In particular, the tensile strength of the SWNT/PVA composite fiber was increased by 1.56 times through the methanol treatment and slightly by the cross-linking treatment. Both the post-electrospinning treatments decreased the strain to failure for the SWNT/PVA composite nanofibers with a lower strain value for the cross-linked nanofiber mats due to a reduced molecular mobility in the cross-linked polymer network.

To gain better understanding of the SWNT–PVA interaction, we have also performed DMTA measurements for the pure PVA and the SWNT/PVA composite nanofibers. As can be seen in figure 5(a), the introduction of 10 wt% SWNTs into the PVA nanofibers led to an increased dynamic elastic modulus (E'), reflecting an improved thermo-mechanical stability. On the other hand, the loss tangent (tan δ) curve for the pure PVA nanofibers showed three peaks at approximately 48, 74 and 100 °C. The first two peaks are associated with relaxations in amorphous regions of PVA with the higher temperature one known as, α_a relaxation, being assigned to the glass transition temperature (T_g) of PVA, at which the micro-Brownian motions of molecular chains become possible [30, 32]. The relaxation peak at the highest temperature (~100 °C) is due to the β_c relaxation in the crystalline domains of PVA. The tan δ curve of the SWNT/PVA nanofibers showed two peaks associated with the α_a and β_c relaxation (figure 5(b)). As expected, the presence of SWNTs in the composite nanofibers led to a small down-shift in T_g temperature (71 °C), and the peak height was also decreased due to a reduced fraction of the polymer matrix and an increased PVA crystallinity. This shift in T_g is consistent with what previously reported for CNT/PVA films [33]. However the peak for the β_c relaxation in the SWNT/PVA nanofibers became broader and shifted to a higher temperature (114 °C), indicating a strong PVA–SWNT interaction in the crystalline region of PVA. A similar observation has also been reported for gel-spun SWNT/PVA composite fibers [34]. The glass transition and β_c relaxation temperatures estimated from the tan δ peaks for both the pure PVA and SWNT/PVA composite nanofibers were listed in table 1.
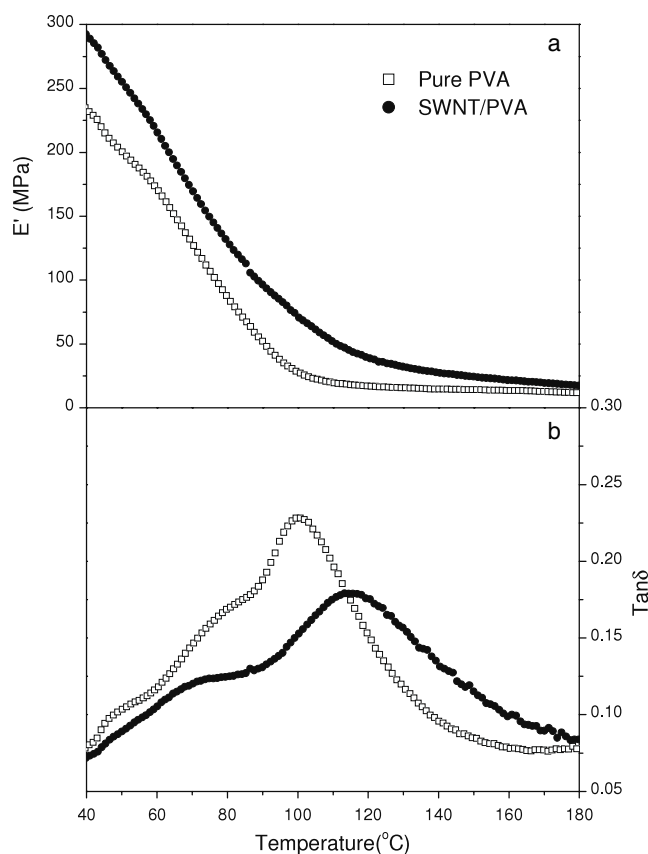

Figure 5. The (a) storage modulus (E') and (b) tan δ of PVA nanofiber and SWNT/PVA composite nanofibers as a function of temperature in tensile mode (frequency = 1 Hz).

The plots of E' and tan δ versus temperature for the SWNT/PVA composite nanofibers before and after the post-electrospinning treatments are depicted in figure 6. As can be seen, the post-treated composite nanofibers showed an increased storage modulus over the entire temperature range studied. The elastic modulus of the composite nanofibers was increased by 2.8 times after the methanol treatment at 40 °C. A similar increase in the elastic modulus of PVA nanofibers after methanol treatment has also been reported previously [35]. The cross-linking reaction increased the E' to 6.2 GPa, which is more than a two fold enhancement compared to the untreated sample. While the SWNT/PVA composite nanofibers treated by either method changed little in the T_g temperature, a noticeable change was observed in the β_c relaxation peak. The observed shift of the β_c relaxation peak to higher temperatures with the post-electrospinning treatments suggested that these treatments enhanced the nanotube–PVA interactions. As the cross-linking reaction decreased the crystallinity of PVA, the lower density of the β_c relaxation peak for the cross-linked SWNT/PVA composite nanofibers with respect to their methanol treated counterparts (figure 6(b)) suggested that the cross-linking reaction might have converted some crystalline PVA into cross-linked network, which also reduced the mobility of the polymer chains [32].

The above DMTA measurements were carried out at a frequency of 1 Hz. We have conducted similar DMTA
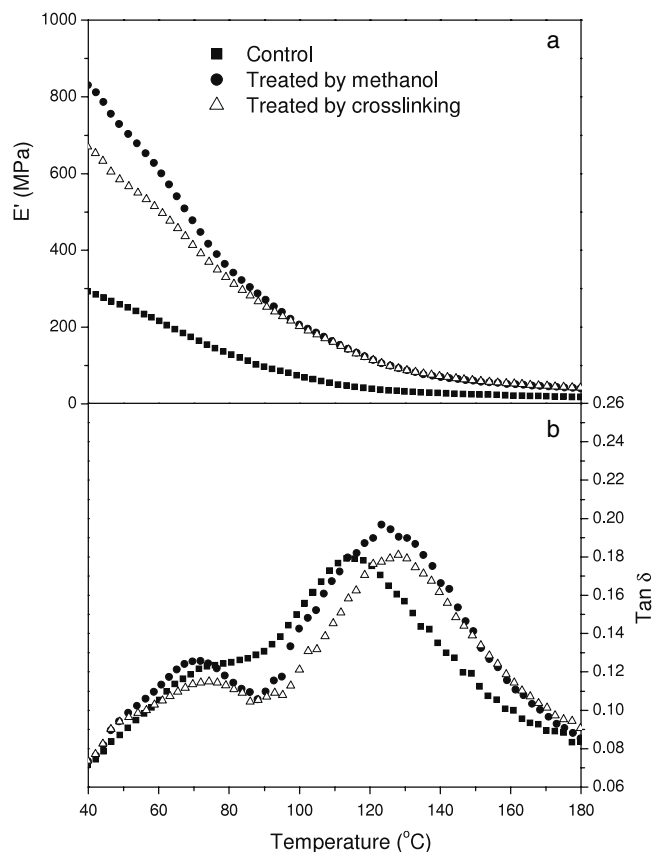
Figure 6. Effect of post-spinning treatments on temperature-viscoelastic properties of SWNT/PVA composite nanofibers: (a) storage modulus; (b) loss tangent.

Figure 7. Dependency of T_g and T_β on the frequency.

measurements at different frequencies and obtained the frequency dependency of T_g and T_β (figure 7). For the pure PVA nanofibers either before or after the post-electrospinning treatments, the value of T_β increased slightly with the frequency. With the increase in the frequency, the T_g temperature for the control PVA and cross-linked PVA nanofibers was slightly reduced, while for the methanol treated one the T_g was slightly higher at higher frequencies. The different trends of T_g for different frequencies suggested that the amorphous region of PVA for the methanol treated samples could have different characteristic to the untreated control sample or cross-linking treated one. For the SWNT/PVA composite nanofibers either before or after the post-electrospinning treatments, the value of T_β increased slightly with the frequency, so did the T_g.

Based on the above tests, the activation energy (E_a) associated with the observed relaxations can be calculated according to the following equation [36]:

$$\ln f = \ln A - \frac{E_a}{RT} + \ln F(\alpha) \qquad (1)$$

where, f, A, E_a and R are frequency, the frequency-related factor, the activation energy, and gas constant, respectively [36–38]. $F(\alpha)$ is the dependency of the relaxation on the frequency. By plotting the $\ln f$ versus $1/T$, we can obtain E_a even without knowing the function $F(\alpha)$.
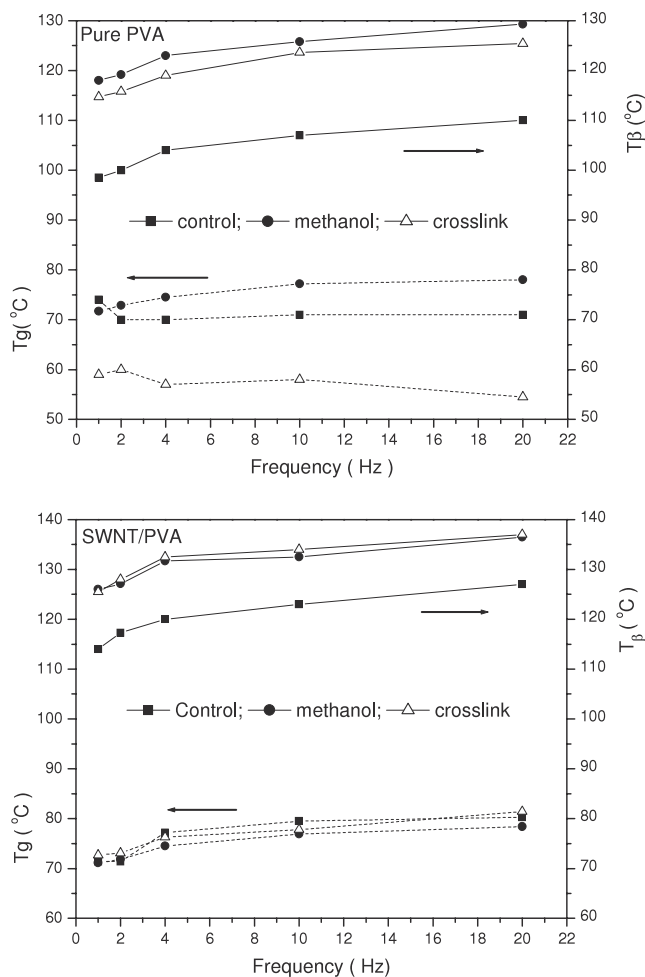
Figure 8 shows $\ln f \sim 1/T$ plots for the pure PVA nanofibers and the SWNT/PVA composite nanofibers. Both the $\ln f \sim 1/T_g$ and $\ln f \sim 1/T_\beta$ showed a linear relationship, indicating a good fit to equation (1). From figure 7, E_a for the α relaxation of the pure PVA nanofibers is estimated to be 41.6 kJ mol^{-1}, which was increased up to 115.9 kJ mol^{-1} for the SWNT/PVA composite nanofibers. These results confirmed that the mobility of the PVA chains in amorphous region was restricted by the presence of SWNTs due to the increased crystallinity, as previously observed for silica/PVA composites [38]. For the β relaxation, the E_a values for the pure PVA nanofibers and the SWNT/PVA composite nanofibers are 128.6 and 133.4 kJ mol^{-1}, respectively. These values are consistent with the higher PVA crystallinity associated with the SWNT/PVA composite nanofibers, which hindered the relaxation movement of the PVA chains, and hence a higher activation energy.

The post-electrospinning treatments increased the E_a values of α relaxation for the pure PVA nanofibers. As can be seen in table 1, the activation energy for the methanol treated PVA nanofibers is more than four times higher than that of the non-treated pure PVA nanofibers. This indicates that the methanol treatment significantly increased the crystallinity. Similarly, the cross-linking reaction also increased the E_a
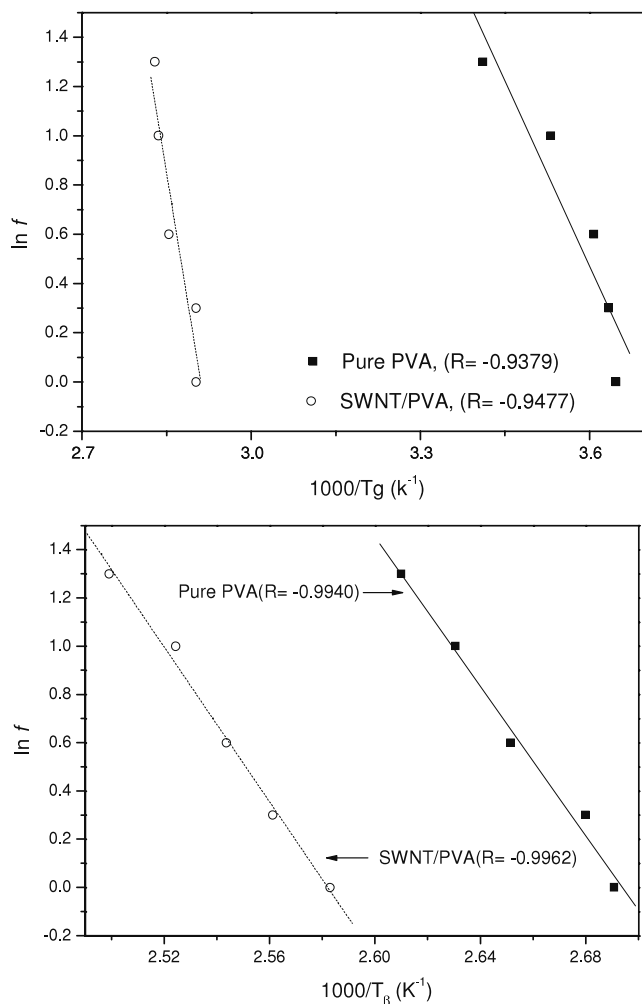
Figure 8. Relationships between logarithmic frequency and reciprocal glass transition temperature and β transition temperature.

value, and both post-electrospinning treatments increased the activation energy for the β relaxation too. Similar results were observed for the SWNT/PVA composite nanofibers, albeit to a less extent.

4. Conclusions

We have demonstrated that the presence of SWNTs in electrospun PVA nanofibers has a profound inference on the morphology of the PVA phase. It was found that SWNTs caused an apparent increase in the PVA crystallinity, and shifted the main crystalline from (100) to (101) phase with a considerably reduced crystalline domain size. This, in turn, changes the tensile strength and surface hydrophobicity of nanofiber mats. The tensile strength of the nanofiber mat can be further improved through post-electrospinning treatments to increase polymer crystallinity by either methanol treatment or cross-linking the PVA composition with glutaric dialdehyde. Dynamic mechanical analyses suggest that the SWNT–PVA interaction occurs mainly in the crystalline domains, while this interaction can be further enhanced via treatment of the nanofiber with methanol and cross-linking of PVA.

References

[1] Cadek M, Coleman J N, Barron V, Hedicke K and Blau W J 2002 *Appl. Phys. Lett.* **81** 5123–5
[2] Coleman J N, Blau W J, Dalton A B, Muñoz E, Collins S, Kim B G, Razal J, Selvidge M, Vieiro G and Baughman R H 2003 *Appl. Phys. Lett.* **82** 1682–4
[3] Kilbride B E, Coleman J N, Fournet P, Cadek M, Drury A and Blau W J 2002 *J. Appl. Phys.* **92** 4024–30
[4] Sandler J K W, Kirk J E, Kinloch I A, Shaffer M S P and Windle A H 2003 *Polymer* **44** 5893–9
[5] Biercuk M, Liaguno M C, Radosavljevic M, Hyun J K, Fischer J E and Johnson A T 2002 *Appl. Phys. Lett.* **80** 2767–9
[6] Wei C, Srivastava D and Cho K 2002 *Nano Lett.* **2** 647–50
[7] Vigolo B, Nicaud A P, Coulon C, Sauder C, Pailler R, Journet C, Bernier P and Poulin P 2000 *Science* **290** 1331
[8] Tang B Z and Xu H 1999 *Macromolecules* **32** 2569
[9] Qian D, Dickeya E C, Andrews R and Rantell T 2000 *Appl. Phys. Lett.* **76** 2868–70
[10] Potschke P, Fornes T D and Paul D R 2002 *Polymer* **43** 3247–55
[11] Sen R, Zhao B, Perea D, Itkis M E, Hu H, Love J, Bekyarova E and Haddon R C 2004 *Nano Lett.* **4** 459–64
[12] Ko F, Gogotsi Y, Ali A, Naguib N, Ye H, Yang G, Li C and Wilis P 2003 *Adv. Mater.* **15** 1161–5
[13] Dror Y, Salalha W, Khalfin R L, Cohen Y, Yarin A L and Zussman E 2003 *Langmuir* **19** 7012–20
[14] Gao J, Yu A, Itkis M E, Bekyarova E, Zhao B, Niyogi S and Haddon R C 2004 *J. Am. Chem. Soc.* **126** 16698–9
[15] Salalha W, Dror Y, Khalfin R L, Cohen Y, Yarin A L and Zussman E 2004 *Langmuir* **20** 9852–5
[16] Vigolo B, Poulina P, Lucas M, Launois P and Bernier P 2002 *Appl. Phys. Lett.* **81** 1210–2
[17] Zhang X, Liu T, Sreekumar T V, Kumar S, Moore V C, Hauge R H and Smalley R E 2003 *Nano Lett.* **3** 1285–8
[18] Probst O, Moore E M, Resasco D E and Grady B P 2004 *Polymer* **45** 4437–43
[19] Cadek M, Coleman J N, Ryan K P, Nicolosi V, Bister G, Fonseca A, Nagy J B, Szostak K, Beguin F and Blau W 2004 *Nano Lett.* **4** 353–6
[20] Chen W, Tao X, Xue P and Cheng X 2005 *Appl. Surf. Sci.* **252** 1404–9
[21] Ryan K P, Cadek M, Drury A, Ruether M, Blau W J and Coleman J N 2005 *Fullerenes Nanotubes Nanostruct.* **13** 431–4
[22] Ciambelli P, Sarno M, Gorrasi G, Sannino D, Tortora M and Vittoria V 2005 *J. Macromol. Sci.* B **44** 779–95
[23] Minus M L, Chae H G and Kumar S 2006 *Polymer* **47** 3705–10
[24] Bin Y, Mine M, Koganemaru A, Jiang X and Matsuo M 2006 *Polymer* **46** 1308–17
[25] Naebe M, Lin T, Tian W, Dai L and Wang X 2007 *Nanotechnology* **18** 225605
[26] Extrand C W 2003 *Langmuir* **19** 646
[27] Rosa M J and Pinho M N D 1997 *J. Membr. Sci.* **131** 167
[28] Hyder M N, Huang R Y M and Chen P 2006 *J. Membr. Sci.* **283** 281–90
[29] Assender H E and Windle A H 1998 *Polymer* **39** 4295–302
[30] Nishio Y and Manley R S 1998 *Macromolecules* **21** 1270–7

[31] Suryanarayana C and Norton M G 1998 *X-Ray Diffraction: A Practical Approach* (New York: Plenum) p 212
[32] Park J-S, Park J-W and Ruckenstein E 2001 *J. Appl. Polym. Sci.* **82** 1816–23
[33] Shaffer M S P and Windle A H 1999 *Adv. Mater.* **11** 937–41
[34] Zhang X, Liu T, Sreekumar T V, Kumar S, Hu X and Smith K 2004 *Polymer* **45** 8801–7
[35] Yao L, Haas T W, Guiseppi-Elie A, Bowlin G L, Simpson D G and Wnek G E 2003 *Chem. Mater.* **15** 1860–4
[36] Varley R J, Hodgkin J H, Hawthorne D G, Simon G P and McCulloch D 2000 *Polymer* **41** 3425–36
[37] Varley R J, Hawthorne D J, Hodgkin J H and Simon G P 1996 *J. Appl. Polym. Sci.* **60** 2251
[38] Peng Z, Kong L X and Li S D 2005 *Synth. Met.* **152** 25–8